universe

MDPI

Article

Possibilities of Detecting Light Dark Matter Produced via Drell-Yan Channel in a Fixed Target Experiment

Eduard Ursov [1,2,*], Anna Anokhina [1,2], Emil Khalikov [2], Ivan Vidulin [1] and Tatiana Roganova [2]

[1] Department of Physics, Federal State Budget Educational Institution of Higher Education, M.V. Lomonosov Moscow State University, 1(2), Leninskie gory, GSP-1, 119991 Moscow, Russia; anokhannamsu@gmail.com (A.A.); vidulin.id18@physics.msu.ru (I.V.)

[2] Skobeltsyn Institute of Nuclear Physics (SINP MSU), Federal State Budget Educational Institution of Higher Education, M.V. Lomonosov Moscow State University, 1(2), Leninskie gory, GSP-1, 119991 Moscow, Russia; nanti93@mail.ru (E.K.); rogatm@yandex.ru (T.R.)

* Correspondence: ursovharleey@mail.ru

Abstract: This work presents the complete modeling scheme of production and detection of two types of light dark matter (LDM) — Dirac fermionic and scalar particles — in a fixed target experiment using SHiP experiment as an example. The Drell-Yan process was chosen as a channel of LDM production; the deep inelastic scattering on lead nuclei was simulated and analyzed in the detector; the production of secondary particles was modeled with the aid of PYTHIA6 toolkit. Obtained observable parameters of secondary particles produced in events associated with LDM were compared with the background neutrino events that were simulated using GENIE toolkit. The yield of LDM events was calculated with various model parameter values. Using machine learning methods, a classifier that is able to distinguish LDM events from neutrino background events based on the observed parameters with high precision has been developed.

Keywords: light dark matter; beam dump experiment; BSM

Citation: Ursov, E.; Anokhina, A.; Khalikov, E.; Vidulin, I.; Roganova, T. Possibilities of Detecting Light Dark Matter Produced via Drell-Yan Channel in a Fixed Target Experiment. *Universe* **2021**, *7*, 33. https://doi.org/10.3390/universe7020033

Academic Editor: Mario Merola and Sabino Meola

Received: 23 December 2020

Accepted: 26 January 2021

Published: 1 February 2021

1. Introduction

Dark matter is a substance which fills the Universe and is invisible in electromagnetic and neutrino radiation but shows itself through gravitational forces . It is used to explain various astrophysical and cosmological phenomena such as distinctive shapes of the rotation curves of galaxies, dynamics of galaxy clusters, and effects of gravitational lensing.

Cross section of non-gravitational interaction of hypothetical dark matter particles with Standard Model (SM) matter has to be extremely small, which is why these particles are called feebly interacting particles (FIPs) [1]. In this work we consider FIPs with masses of approximately 1 GeV as light dark matter (LDM) [2]. The models describing LDM require the existence of mediators, special particles [3], through which LDM interacts with baryonic matter.

There are many experiments aiming at detecting dark matter through its non-gravitational interaction with SM matter. Neutrino fixed target experiments with high luminosity (MiniBooNE [4] and T2K [5]) are of particular interest for LDM studies. One of the tasks of the upcoming SHiP experiment [6] at CERN, which will use a proton beam with incident energy of 400 GeV, is LDM detection.

In this work a full simulation of LDM events and neutrino background events in a fixed target experiment with characteristics similar to the SHiP experiment was carried out, so let us provide a brief description of this experiment. The defining parameter for fixed target experiments is POT (protons on target), its value has a direct influence on the sensitivity of an experiment to signal events. For SHiP POT will be $2 \cdot 10^{20}$ during the first five years of its work.

The main steps of production and detection of LDM and neutrinos in the SHiP experiment are as follows. A 400 GeV proton beam collides with a hybrid target made of

tungsten and molybdenum. As a result of the collision of the proton beam with target nuclei, secondary particles (in particular, LDM and neutrino) are produced. Secondary hadrons and muons are slowed down and deflected along the way to the detector with the help of various protective systems. Then, LDM and neutrinos reach an emulsion neutrino detector named SND (Scattering and Neutrino Detector). SND is based on the Emulsion Cloud Chamber technique and consists of a sequence of passive material (lead) plates, between which emulsion films are inserted. This technology has already proved itself in the OPERA experiment, which studied neutrino oscillations [7]. The main advantage of the emulsion detector is its high spatial resolution, which allows one to obtain a precise 3-dimensional reconstruction of the event down to several microns. LDM particles as well as neutrinos are considered to have a very small interaction cross section, thus, the neutrino detector will be suitable for LDM detection as well. Secondary particles produced in the SND will form tracks in emulsion films. Analysis of these tracks will enable the reconstruction of primary particles.

The main task of this work is to continue the discussion presented in [8]. The paper is organized as follows: in Section 2 we discuss the Light Dark Matter model and the Drell-Yan cross section properties. The simulation steps with LDM features, LDM deep inelastic scattering and secondary particle production are described in Section 3. Neutrino event simulation procedure done with the help of GENIE generator is presented in Section 4 (see [9]). It is important to obtain the LDM signatures in the SND detector and compare them to background neutrino events. Such signatures are presented in Section 5. The sensitivity of our LDM production and detection scheme are discussed in Section 6. The results of LDM event selection are also shown there. Finally, we conclude in Section 7.

2. Light Dark Matter Model

We consider an LDM candidate for dark matter, which is a FIP with mass of about 1 GeV. An additional particle is introduced along with LDM: a light mediator through which LDM can annihilate and interact with SM matter (see [10,11]). Otherwise, there would have been too much LDM in the early Universe, which would contradict the current estimates of the density of matter in the Universe. A light vector mediator is introduced as a so-called dark photon V (sometimes denoted as A') associated with $U(1)^{'}$. The dark photon is kinetically mixed with the SM $U(1)$ gauge bosons (γ^*/Z) with field strength $F_Y^{\mu\nu}$ via the coupling ϵ (called kinetic mixing coefficient), thus ensuring the interaction between LDM and SM particles [12].

Let us define a Lagrangian corresponding to LDM (χ), a fermion or a scalar, and a dark photon V [13]:

$$L = L_\chi - \frac{1}{4} V_{\mu\nu} V^{\mu\nu} + \frac{1}{2} m_V^2 V_\mu V^\mu - \frac{\epsilon}{2} V_{\mu\nu} F_Y^{\mu\nu}, \text{ where} \tag{1}$$

$$L_\chi = \begin{cases} i\bar{\chi} \not{D} \chi - m_\chi \bar{\chi} \chi, \text{ (Dirac fermion)} \\ |D_\mu \chi|^2 - m_\chi^2 |\chi|^2, \text{ (complex scalar).} \end{cases} \tag{2}$$

Here m_V is the mass of the dark photon and $D_\mu = \partial_\mu - i g_D V_\mu$ is a covariant derivative. Let us also define the parameters of the light dark matter model:

- two types of LDM will be considered: the Dirac fermion and the complex scalar;
- the range of dark photon masses to be studied is 0.6–3 GeV;
- the range of the kinetic mixing coefficient $\epsilon = 10^{-4}$–1 and the range of the coupling constant for the dark sector α_D = 0.1–1.0.

2.1. LDM Generation

Several mechanisms for generating dark photons and LDM are assumed. Depending on the energy of the incoming proton beam and the selected model parameters, different channels of dark photon generation can be realized taking into account the

kinetic mixing of the dark photon with the SM photon and the subsequent decay of the dark photon into a pair of LDM particles [14]. They are:

- a meson ($\pi^0/\eta/\rho$) decay. This channel is dominant for light LDM and mediators. The production occurs through the decay of a meson:

$$\pi^0/\eta/\rho \to \gamma + V^* \to \gamma + \chi + \chi^\dagger \tag{3}$$

- proton bremsstrahlung

$$p + N \to p + N + V^* \to p + N + \chi + \chi^\dagger, \tag{4}$$

- the Drell-Yan process
  The Drell-Yan process begins to dominate at high energies of the incident beam and with large masses of the dark photon:

$$p + N \to V^* \to \chi + \chi^\dagger. \tag{5}$$

  It is schematically shown in Figure 1.

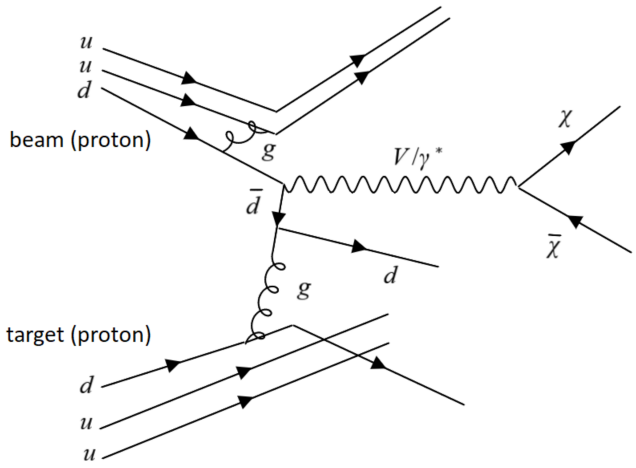

Figure 1. Scheme of the Drell-Yan process with the production of an LDM pair.

Let us focus on the Drell-Yan channel [15]. For mediator masses greater than 1 GeV this process will dominate as shown in [16]. In a fixed target experiment, the collision of a high-energy proton with a proton or a neutron of the target results in the annihilation of a quark-antiquark pair, thus producing an SM hypercharge γ^*/Z that is kinetically mixed with a dark photon, which then decays into an LDM pair.

The kinematics of the Drell-Yan process are often used for collider experiments. For the version of the fixed target experiment considered by us one can easily obtain 4-momenta of LDM particles produced in the decay of a dark photon in the laboratory frame using several successive Lorentz transformations (Figure 2):

$$\begin{cases} E_{V_1} = \gamma_c \gamma_q m_V (1 + \beta_c \beta_q) \\ p_{V_1} = \gamma_c \gamma_q m_V (\beta_c + \beta_q), \end{cases} \tag{6}$$

$$\gamma_c = \frac{1}{1 - \beta_c^2} = \frac{\sqrt{p_b^2 + m_p^2}}{m_p}, \tag{7}$$

$$\beta_q = \frac{(x - \frac{\tau}{x}) p_b}{2 m_V}, \tag{8}$$

where x is the ratio between the quark momentum and the total proton momentum, $\tau = \frac{m_v^2}{s}$, while the $\sqrt{s}$ is the energy in the center of mass system.

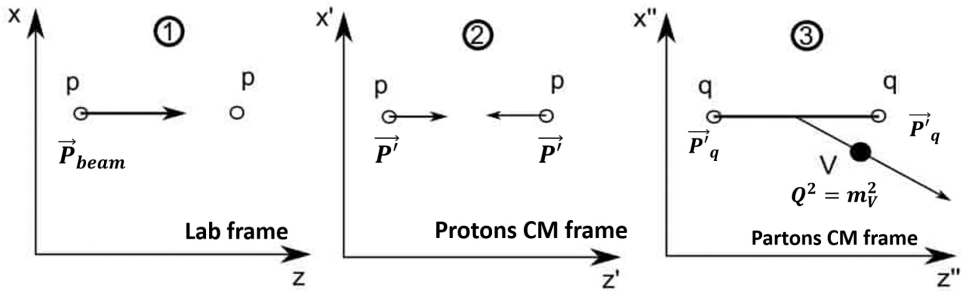

Figure 2. Proton-proton collisions in the target shown in three different reference systems.

The cross section of the Drell–Yan process is calculated using the following formula (see e.g., [14]):

$$\sigma(pN \to V) = \frac{4\pi^2\epsilon^2\alpha_{em}}{m_V^2} \sum_q Q_q^2 \int_\tau^1 \frac{dx}{x} \tau \left[f_{q/p}(x) f_{\bar{q}/p}\left(\frac{\tau}{x}\right) + f_{\bar{q}/p}(x) f_{q/p}\left(\frac{\tau}{x}\right) \right], \quad (9)$$

where $f_{q/p}(x)$ are parton distribution functions for tungsten (target) and proton (CTEQ6.6 PDFs [17] were used).

The dependence of this cross section on the dark photon energy in the laboratory frame for different masses of the dark photon is shown in Figure 3. The energy of the incoming proton beam is 400 GeV.

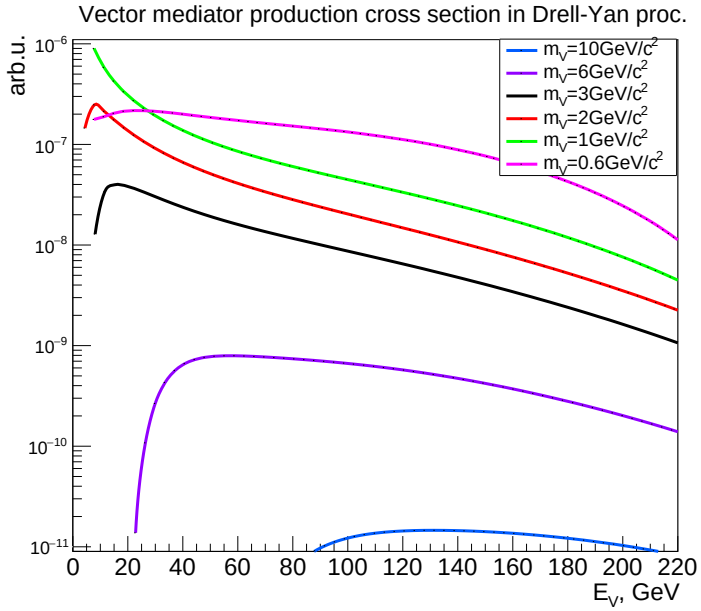

Figure 3. Dependence of the differential cross section of the Drell-Yan process on the energy of the generated mediator (dark photon) for different masses of the mediator.

Based on Figure 3, it can be concluded that with an increase in the mass of the mediator the cross section decreases and shifts a little to the region where more energetic mediators are produced. This result will be useful in the upcoming SND@LHC experiment [18]. For LHC energies an increase in the cross section of the production of LDM with large masses (4–6 GeV) is expected.

The obtained relations for the 4-momentum of the produced mediator and the cross section of its production are used in modeling LDM events.

The dark photon is expected to decay into a pair of particles. There are several decay channels for which the main condition is $m_V > 2m_{particles}$. The decay widths for these channels are (see [3,19]):

$$\Gamma(V \to \overline{\chi}\chi) = \frac{\alpha_D}{3} m_V \left(1 + \frac{2m_\chi^2}{m_V^2}\right) \sqrt{1 - \frac{4m_\chi^2}{m_V^2}}, \tag{10}$$

$$\Gamma(V \to l^- l^+) = \frac{\alpha_{em}\epsilon^2}{3} m_V \left(1 + \frac{2m_l^2}{m_V^2}\right) \sqrt{1 - \frac{4m_l^2}{m_V^2}}. \tag{11}$$

Figure 4 shows the dependencies of the dark photon mean free path from its production to its decay into an LDM pair (left) and a lepton ($\mu^-\mu^+$) pair (right) depending on the values of model parameters. It is clearly seen that the process of dark photon decay into an LDM pair will dominate.

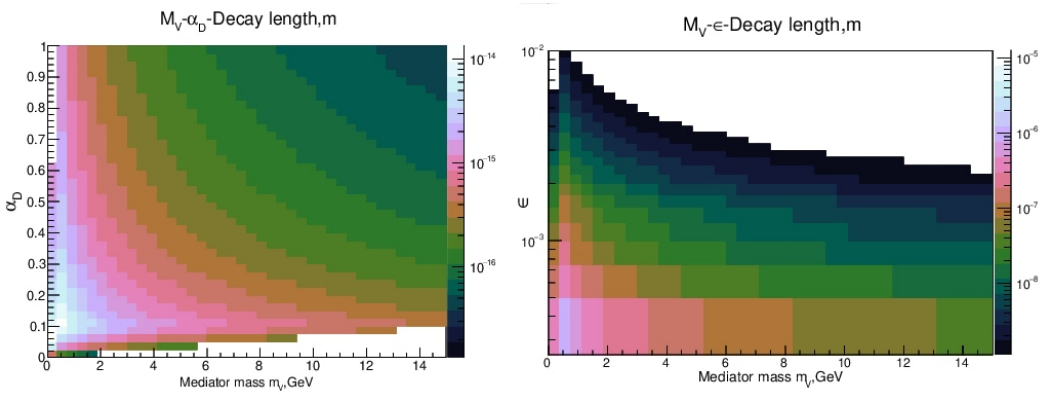

Figure 4. Dependence of the dark photon mean free path from its production to its decay into an LDM pair (left) and a $\mu^-\mu^+$ pair (right) on the dark photon mass and parameters α_D and ϵ.

2.2. Interaction of LDM with the Detector Material

Let us consider the mechanisms of LDM particle – SM particle interaction. There are three channels of interaction [14]: elastic scattering on electrons or nuclei, quasi-elastic scattering and deep inelastic scattering (DIS) on nuclei. DIS channels on nuclei and electron scattering will be of particular interest for the SHiP's energy range. In this paper we consider DIS on nuclei.

3. Simulation Steps

The simulation of the events involving LDM production and interaction with the detector has been done in several steps outlined in Figure 5. Background neutrino events were simulated using the GENIE generator [9]. Our objective was to obtain and analyze kinematic features of all the intermediary and final state particles based on the complete set of cross sections for the LDM interaction processes, as well as to set the criteria for LDM event selection in the detector. PYTHIA6 toolkit [20] was utilized during the final step of our simulation. The steps of our simulation are associated to the following consecutive tasks:

1. Dark photon production through the Drell–Yan process after the collision of an incident proton with a tungsten target;
2. Dark photon decay and selection of LDM particles that have reached the detector;
3. Deep inelastic scattering of LDM particles on lead target nuclei;
4. Production of secondary particles (i.e., hadronization) as a result of DIS.

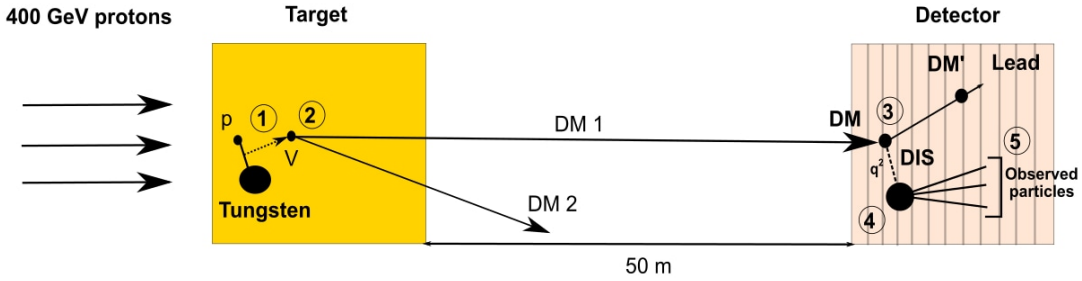

Figure 5. Simulation scheme.

3.1. LDM Production

We have obtained a set of dark photons with energies and momenta distributed in accordance with the cross section described by Equation (9). After dark photons (mediators) are produced, they create LDM pairs following the rules of massive relativistic particle decay to two particles of equal masses. The directions of secondary LDM particles are simulated according to angular distributions corresponding to (a) production of scalar dark matter (DM) particles from a vector dark photon and (b) production of fermionic DM particles from a vector dark photon. For scenario (a) DM particles will be distributed in a mediator rest frame as $g(cos\theta) = \frac{3}{4}(1 - cos^2\theta)$, while for scenario (b) the distribution will be $g(cos\theta) = \frac{3}{8}(1 + cos^2\theta)$. Energy distributions of fermionic and scalar LDM particles with different masses produced in the target and reaching the detector are shown in Figure 6. It should be noted that the number of LDM particles in the detector decreases significantly with the increasing LDM masses. This circumstance is very important for the correct estimation of the detector sensitivity.

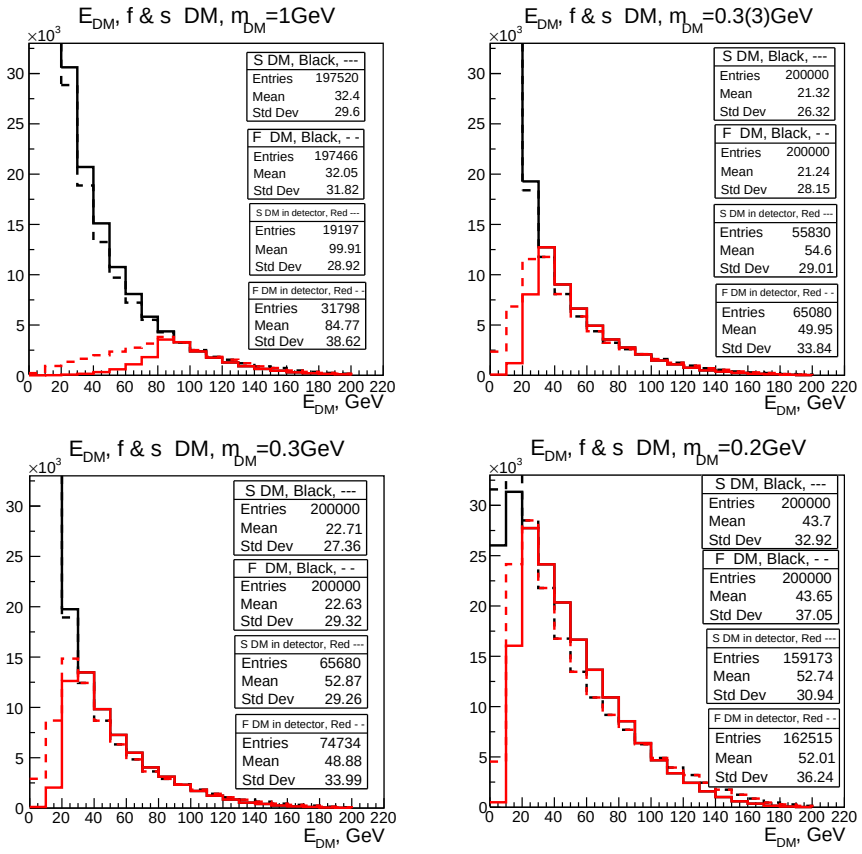

Figure 6. Energy E distributions of simulated LDM particles with various masses produced in the target and reaching the SND detector.

Energy and pseudorapidity distributions of simulated LDM particles (both fermionic and scalar) reaching the detector are shown in Figure 7 for a mediator mass 3 GeV.

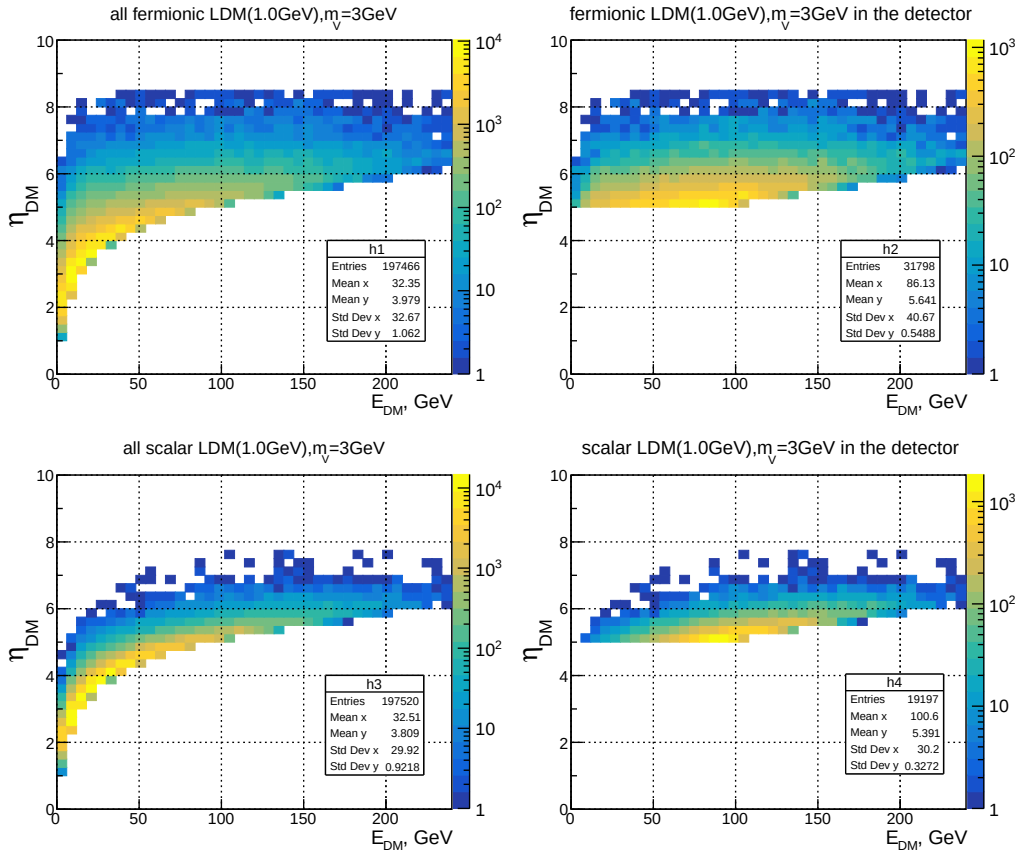

Figure 7. Pseudorapidity η and energy E distributions of simulated LDM particles reaching the SND detector.

Nonzero spin leads to a wide range of pseudorapidities for the case of fermionic LDM. However, their energy distribution does not change substantially in comparison with the case of scalar LDM.

3.2. Deep Inelastic Scattering of LDM in the Detector

A formula for DIS cross section in the case of fermionic LDM was adopted from [21], while scalar LDM cross section was calculated by us (see Appendix A, which also provides the constraints on kinematic parameters). The cross sections are defined as follows:

$$d\sigma_{ferm} = \pi\alpha_{em}\alpha_D\epsilon^2 \frac{d\nu dQ^2}{E^2 - m_\chi^2} \frac{\nu}{(Q^2 + m_v^2)^2} \left[\frac{(2E-\nu)^2}{\nu^2 + Q^2} + \frac{Q^2 - 4m_\chi}{Q^2}\right] \sum_q x_{\mathrm{bj}} f_{q/A}(x_{\mathrm{bj}}, Q^2), \quad (12)$$

$$d\sigma_{sca} = \pi\alpha_{em}\alpha_D\epsilon^2 \frac{d\nu dQ^2}{E^2 - m_\chi^2} \frac{\nu}{(Q^2 + m_v^2)^2} \left[\frac{(2E-\nu)^2}{\nu^2 + Q^2} - \frac{2Q^2 + 4m_\chi}{Q^2}\right] \sum_q x_{\mathrm{bj}} f_{q/A}(x_{\mathrm{bj}}, Q^2). \quad (13)$$

Figure 8 shows the dependence of DIS cross sections on squared transferred momentum Q^2 for fermionic and scalar LDM and various values of energy lost by LDM during its interaction with a target nucleus: $\nu = E - E'$. It can be concluded that the DIS cross sections at high values of transferred momentum are practically independent of spin; the spin dependence starts to show itself only at ν values of about 20 GeV.

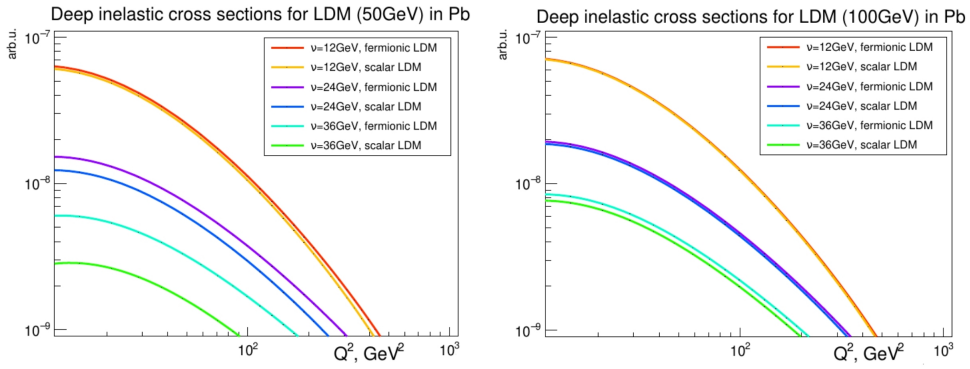

Figure 8. DIS cross sections for LDM with energies 50 GeV (left) and 100 GeV (right) in lead.

3.3. Production of Secondary Particles in DIS Processes inside the Detector

For every LDM particle reaching the emulsion detector we calculate the values of kinematic parameters Q^2 and ν according to cross sections described by Equations (12) and (13). The Q^2 distributions for the simulated fermionic and scalar LDM events with different masses ($m_\chi = 0.2, 0.33, 1.0$ GeV) are shown in Figure 9. In order to simulate the production of secondary particles in the detector, we used PYTHIA6 toolkit. PYTHIA6 allows one to control many parameters of simulated processes, which can be used to make simulated hadronization processes as much consistent with the LDM interaction scenarios as possible.

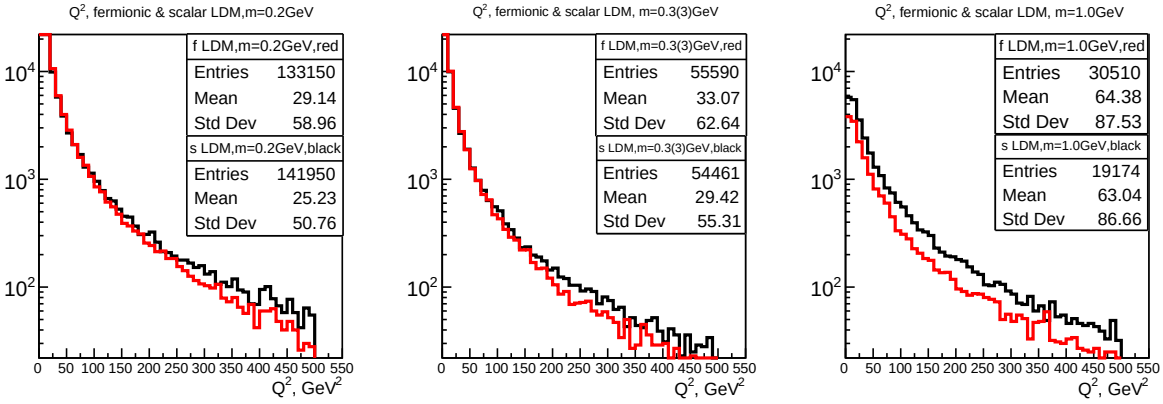

Figure 9. Q^2 distributions for fermionic and scalar LDM particles with different masses.

As a hadronization model we utilized a model of electroweak scattering of an abstract lepton with masses 0.2 and 1 GeV enabling various $(\gamma^*/Z)\gamma$ physical processes from [20].

Particular processes were chosen for each event in accordance with the maximum calculated cross section. To simulate the transfer of a particular value of Q^2 we used PYTHIA6 because it enabled us to put kinematic constraints.

4. Simulation of Neutrino Events

It is vital for the experiment to understand what are the sources of background events and how to distinguish DM events from the background ones. The main sources of background in our case are:

- neutrino events;
- DIS of muons in the detector;
- muons produced in the atmosphere by cosmic rays.

Muon background could be reduced through the improvement of an active shielding system; muons from cosmic rays have specific energies and come from specific directions. That leaves the neutrino background, which we discuss below.

When neutrinos interact with target nuclei or electrons of the detector through charged current (CC), the main signature of a neutrino event is the production of a high-energy charged lepton, which wouldn't be present in the case of an LDM event. This charged lepton would be most likely identified in ECC.

However, in the case of a neutral current (NC) interaction the identification of background neutrino events is a bit more complicated. For neutrinos scattering on electrons it is still possible to simulate the spectra and understand that LDM particles (which have higher masses then neutrinos) contribute to the recoil electron's energy. But for the case of DIS of neutrino on nuclei one should carry out a thorough research to create specific criteria for distinguishing LDM events from neutrino background events.

In this paper we used GENIE Monte-Carlo generator to simulate neutrino interactions with the material of the detector. Energy spectra of neutrinos produced in the target and reached the detector, were taken from [6].

Full modeling of neutrino events consists of several steps:

1. Obtaining the spectra of neutrinos reaching the detector;
2. Calculating cross sections of interactions of 0–150 GeV neutrinos of various flavors with lead nuclei at energies 0–150 GeV;
3. Simulating interactions of neutrinos of various flavors with lead nuclei in the detector.

For DIS modeling at high energies GENIE uses the so-called Bodek–Yang model, for hadronization modeling—«AGKY» model [22], which, in turn, utilizes PYTHIA6 in the total invariant system mass range $W > 3$ GeV.

GENIE provides precalculated cross sections of neutrino interactions for energies up to 100 GeV. In order to simulate the processes with high energies, one has to obtain the splines of corresponding cross sections. We calculated cross sections of neutrinos of three different flavors in the 0–150 GeV energy range using the 'gmsksplʼ command embedded in the GENIE code.

Using the obtained cross sections, we have simulated neutrino background events.

5. Comparison of LDM and Neutrino Events

Hadronization in LDM and Neutrino Events

About 10^5 LDM and neutrino events producing secondary particles were obtained. To set the selection criteria used for distinguishing the LDM events from the neutrino background, it is necessary to analyze various parameters that can be obtained in the experiment. The kinematic parameters of charged particles were considered, since these parameters can be reconstructed from the visible tracks left by such particles in the SND emulsion detector.

The first two parameters that we analyzed are the invariant mass of a system of charged particles in the event M_{inv}^{ch} and the total transverse momentum of the event P_T. Figure 10 shows the distributions of P_T of charged particles both in the events associated with scalar and fermionic LDM particles and in the neutrino ones, and the distributions of M_{inv}^{ch} of charged particle systems for the same events.

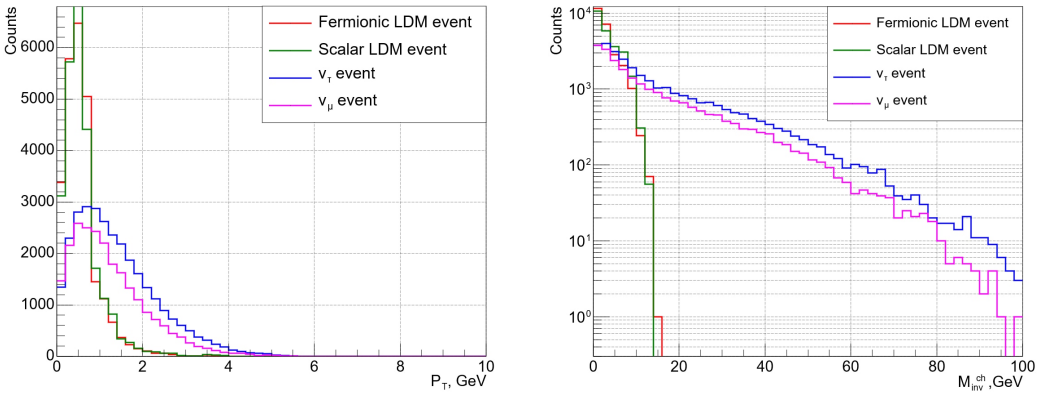

Figure 10. Distributions of the total transverse momenta and invariant mass of a system of charged secondary particles in an event for scalar and fermionic LDM, ν_τ and ν_μ.

The fat-tailed distribution of M_{inv}^{ch} for neutrino events can be explained by a large number of quasi-elastic collisions of ν_τ (as well as ν_μ) with lead nuclei. In these collisions the nuclei decay into nucleons, which corresponds to smaller values of Q^2 compared to LDM.

The next two parameters we considered were the total energy and pseudorapidity of the charged particle system in the event. Figure 11 shows the two-dimensional histogram (heatmap) for the parameter distributions of LDM and neutrino events (distributions for scalar and fermionic LDM particles practically overlap, so only events from fermions were shown).

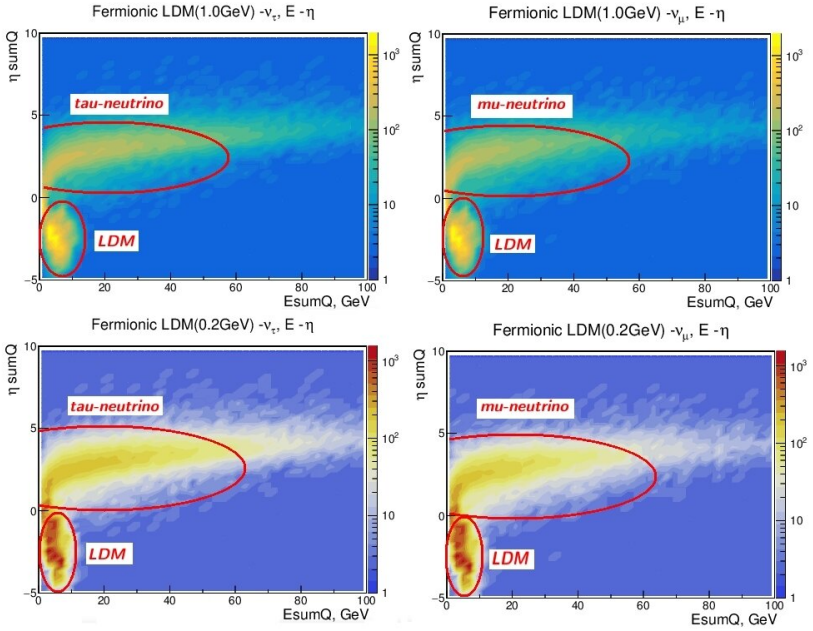

Figure 11. Distributions of the total energies and pseudorapidities of charged particle systems of LDM and neutrino events.

Using machine learning methods, we created a classifier that is able to distinguish LDM events from the background neutrino events based on the observed kinematic parameters with high precision. It is also possible to estimate and constrain the detector sensitivity, which is described in the following section.

6. Event Selection and Detector Sensitivity

6.1. Sensitivity

Using the complete scheme for modeling the events associated with LDM production, we were able to set constraints on the sensitivity of the experiment to the following parameters of the LDM model:

- mixing coefficient ϵ;
- the dark sector coupling strength $\alpha_D = \frac{g_D^2}{4\pi}$;
- dark photon mass m_V ($m_V = 3m_\chi$).

To show the obtained sensitivity we use the (m_V, Y) plane where Y is defined as:

$$Y = \epsilon^2 \alpha_D \left(\frac{m_\chi}{m_V}\right)^4. \tag{14}$$

The parameter Y is linked to the dark matter annihilation cross section via the formula [8,23]:

$$\sigma(\chi\bar{\chi} \to f\bar{f}) v_{rel} \propto \frac{8\pi v_{rel}^2 Y}{m_\chi^2} (\text{if } m_V > 2m_\chi), \tag{15}$$

where v_{rel} is the relative velocity between the colliding dark matter particles.

Figure 12 shows the yield of events from LDM particles which were generated via the Drell–Yan channel and interacted in the detector via the DIS channel with various values of α_D.

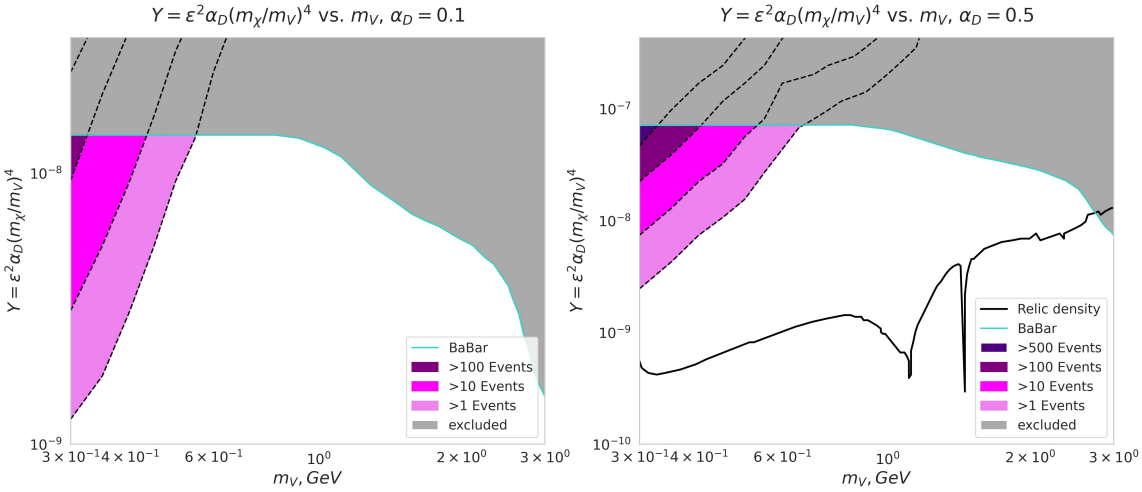

Figure 12. The yield of events from LDM particles which were generated via the Drell-Yan channel and interacted in the detector via the DIS channel with various values of α_D (purple regions). The gray regions are excluded by the existing constraints (e.g., the ones obtained in the BaBar experiment [24]), and the dark curve shows the relic density behavior [23] at various Y and m_V.

We can conclude that the number of events in our scenario will be sufficient at $m_V \simeq 0.3$–0.6 GeV. That range is defined by the geometry of the detector and limited from below by the features of the production mechanism (at low masses of the dark photon m_V the strong coupling α_s is $O(1)$ and the description of the hadrons in terms of constituent partons is spoiled by the confinement) and from above by the existing experimental constraints.

6.2. LDM Event Selection

A naive Bayesian classifier was used to select events. Its main advantages are simplicity of implementation and low computational costs for training and classification. In those

rare cases when features are nearly independent, a naive Bayesian classifier is close to optimal. A sufficiently small amount of data is needed for training, assessment and classification using this algorithm. The implementation was done with the aid of scikit-learn [25] library in Python, assuming that the original parameter distributions were Gaussian.

The precision and recall metrics are usually introduced to evaluate the performance of a machine learning algorithm on each class separately:

$$precision = \frac{TP}{TP + FP}, \tag{16}$$

$$recall = \frac{TP}{TP + FN}, \tag{17}$$

where TP, FP and FN are determined via the error matrix (Figure 13). Precision can be interpreted as the fraction of objects identified as positive by the classifier that are in fact positive (correctly defined), and recall shows what fraction of objects from all objects of a positive class were found by the algorithm.

	$y = 1$	$y = 0$
$\hat{y} = 1$	True Positive (TP)	False Positive (FP)
$\hat{y} = 0$	False Negative (FN)	True Negative (TN)

Figure 13. Error matrix. $\hat{y}$ is the algorithm response to the object, and y is the true class label of this object.

The Precision-Recall (P-R) metric is used to estimate the quality of classifiers in case of very unbalanced classes [26]. We use it to estimate the accuracy of the Bayesian classifier. The P-R curve shows the trade-off between precision and recall for different thresholds. The large area (close to 1) under the curve represents both high recall and high precision. Figure 14 shows the P-R curves for the classes of events from scalar LDM particles, fermionic LDM particles and neutrinos.

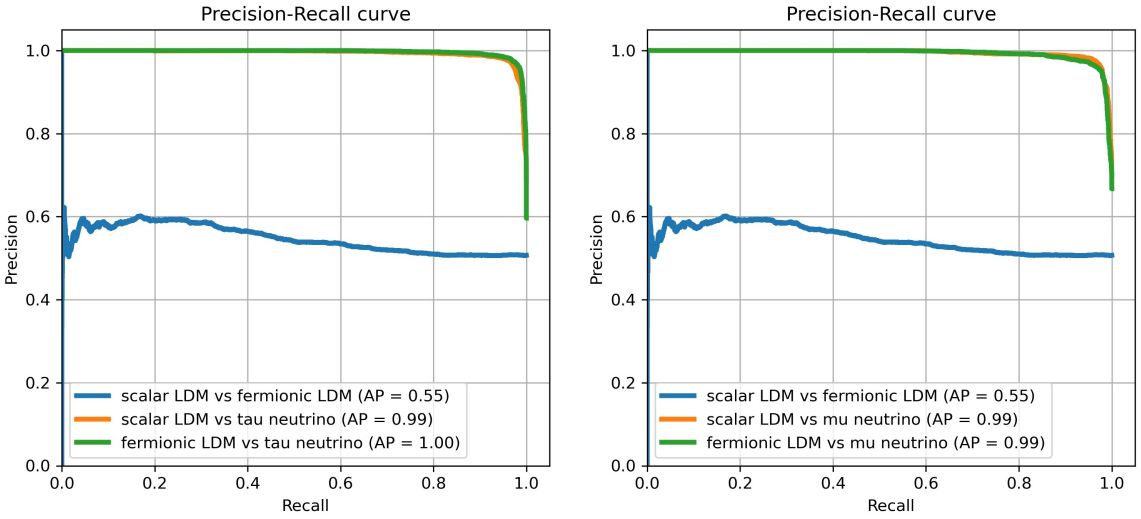

Figure 14. Precision-Recall curves for fermionic and scalar LDM, ν_τ and ν_μ events. The higher the area under the curve, the more accurately the event is classified.

Considering the areas under the curves (AP—average precision in Figure 14) we can conclude that the Bayesian classifier efficiently distinguishes the LDM events from the neutrino background and does a rather poor job in determining whether LDM has spin, since the precision value close to 0.5 is caused by a large number of false positive results.

A simple cut-based event selection procedure (applying cuts to the pseudorapidity η parameter) was tested (Figure 11), and the results were compared with the ones obtained for the case of the developed classifier. In the best case, when 99% of LDM particles are correctly identified, about 6% of neutrino events are classified as LDM, while the Bayesian classifier, in accordance with the P-R curves, shows almost perfect results at any threshold of the classifier (approximately 1% of incorrectly classified events). At this stage, we analyzed the kinematic characteristics of secondary particles produced in the detector and did not consider the tracks of particles in emulsion plates. In case of reconstructing the kinematic characteristics of events from the tracks in emulsions, the developed classifier will have additional advantages over the cut-based event selection procedure.

7. Conclusions

In this work we present a complete scheme for modeling the processes of (a) LDM (light dark matter) production on the SPS beam in the fixed target experiment (e.g., SHiP) via the Drell-Yan channel and (b) the interaction of LDM with the detector material through deep inelastic scattering on lead nuclei. Scalar and fermionic LDM particles with a mass of approximately 1 GeV are considered. We have obtained the expression for the DIS cross section in the case of the scalar LDM particle.

Moreover, we have determined the signatures on the basis of which it is possible to distinguish the events associated with the LDM interactions from the neutrino background events. Constraints on the SHiP detector sensitivity to the parameters of the LDM model were obtained. We can conclude that the number of events in our scenario will be sufficient at $m_V \simeq 0.3$–0.6 GeV.

This scheme of modeling and analysis of events, with the modification of the mediator production cross section, can be applied in experiments at LHC where it is possible to investigate LDM particles with large masses.

Author Contributions: Conceptualization, A.A. and E.U.; methodology, E.U.; software, A.A.; validation, T.R.; formal analysis, I.V.; investigation, E.K.; resources, E.U.; data curation, E.U.; writing—original draft preparation, E.U.; writing—review and editing, A.A.; visualization, E.U.; supervision, T.R.; project administration, T.R.; funding acquisition, E.U. All authors have read and agreed to the published version of the manuscript.

Funding: This research was funded by Basis Foundation grant number #20-2-9-26-1 and by the Interdisciplinary Scientific and Educational School of Moscow University «Fundamental and Applied Space Research».

Acknowledgments: We express our gratitude to A. Pukhov and P. deNiverville for advice on some theoretical issues.

Conflicts of Interest: The authors declare no conflict of interest. The funders had no role in the design of the study; in the collection, analyses, or interpretation of data; in the writing of the manuscript, or in the decision to publish the results.

Appendix A. Calculation of DIS Cross Section of an LDM Particle on a Nucleon

At SHiP energies the deep inelastic interaction channel will dominate. Let us consider the DIS of LDM particles (χ) on lead nuclei in the detector. The χ particle exchanges a virtual mediator V with the nucleus. Particle's momentum before the scattering is equal to p_χ and p'_χ after the scattering. So, the virtual mediator V carries the momentum $q = p_\chi - p'_\chi$, hence the square of transferred momentum is $Q^2 = -q^2$. Let us also define the energy transferred from χ to the nucleon by the mediator $\nu = E - E'$. This energy must be greater than a certain value at which DIS takes place: $\nu > E_{cut}$ [27]. Finally, let us define the Bjorken variable $x_{bj} = \frac{Q^2}{2M\nu}$ (M is the nucleus mass).

Using lowest order perturbation theory, Ref. [21] derived the following expression for the differential cross section in the case of deep inelastic lepton scattering:

$$d\sigma = \frac{\pi\alpha_{em}\alpha_D\epsilon^2}{M}\frac{d\nu dQ^2}{E^2 - m_\chi^2}\frac{L^{\mu\nu}W_{\mu\nu}}{(Q^2 + m_v^2)^2}, \tag{A1}$$

where tensors $L^{\mu\nu}$ and $W_{\mu\nu}$ describe dark and hadronic vertices of diagram on Figure A1. The situation is similar to the DIS of neutrinos on the nucleus. Now let us find these tensors.

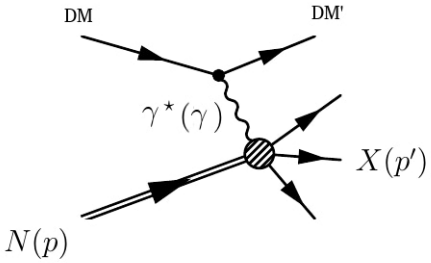

Figure A1. DIS of LDM on nucleus [27].

The hadronic tensor is found using the following formula:

$$W^{\mu\nu} = C_T^{\mu\nu}F_T(x_{bj}, Q^2) + C_L^{\mu\nu}F_L(x_{bj}, Q^2), \tag{A2}$$

where $F_T(x_{bj}, Q^2)$ and $F_L(x_{bj}, Q^2)$ are standard structure functions; C_T corresponds to the exchange of a transversely polarized virtual mediator, and C_L—to a longitudinally polarized one.

The dark sector tensor $L^{\mu\nu}$ can be calculated using the squared diagram [28]:

$$L^{\mu\nu} = \begin{cases} 4p_\chi^\mu p_\chi^\nu - 2(p_\chi^\mu q^\nu - p_\chi^\nu q^\mu) + q^2 g^{\mu\nu} & \text{(fermionic LDM)}, \\ 4p_\chi^\mu p_\chi^\nu - 2(p_\chi^\mu q^\nu - p_\chi^\nu q^\mu) + q^\mu q^\nu & \text{(scalar LDM)}. \end{cases} \tag{A3}$$

Here $g^{\mu\nu}$ is metric tensor.

In the convolution of the hadronic tensor and the dark sector tensor, we obtain the following terms:

$$C_L^{\mu\nu}L_{\mu\nu} = M\nu\frac{4E(E-\nu) - Q^2}{\nu^2 + Q^2}; \tag{A4}$$

$$C_T^{\mu\nu}L_{\mu\nu} = \begin{cases} \frac{Q^2(2E-\nu)^2}{\nu^2+Q^2} + Q^2 - 4m_\chi^2 & \text{(fermionic LDM)}, \\ \frac{Q^2(2E-\nu)^2}{\nu^2+Q^2} - 2Q^2 - 4m_\chi^2, & \text{(scalar LDM)}, \end{cases} \tag{A5}$$

The final step is to calculate the structural functions. They can be obtained as the convolutions of the parton distribution function and the parton structure function $\hat{F_T}$ or $\hat{F_L}$. In the lowest order of the perturbation theory [21]:

$$F_L = 0, \tag{A6}$$

$$F_T = \frac{1}{2x_{bj}}\sum_q x_{bj}f_{q/A}(x_{bj}, Q^2). \tag{A7}$$

The limits of Q^2 and ν are

$$E_{\text{cut}} < \nu < E - m_\chi, \tag{A8}$$

$$Q^2 < 2M\nu. \tag{A9}$$

We used parton distribution functions for the nucleus provided at leading order by Hirai-Kumano-Nagai (HKNlo) [29].

So, the final formulas for the DIS cross section on the lead nucleus of the scalar and fermionic LDM are:

$$d\sigma_{ferm} = \pi\alpha_{em}\alpha_D\epsilon^2 \frac{d\nu dQ^2}{E^2 - m_\chi^2} \frac{\nu}{(Q^2 + m_v^2)^2} \left[\frac{(2E-\nu)^2}{\nu^2 + Q^2} + \frac{Q^2 - 4m_\chi}{Q^2} \right] \sum_q x_{\text{bj}} f_{q/A}(x_{\text{bj}}, Q^2), \tag{A10}$$

$$d\sigma_{sca} = \pi\alpha_{em}\alpha_D\epsilon^2 \frac{d\nu dQ^2}{E^2 - m_\chi^2} \frac{\nu}{(Q^2 + m_v^2)^2} \left[\frac{(2E-\nu)^2}{\nu^2 + Q^2} - \frac{2Q^2 + 4m_\chi}{Q^2} \right] \sum_q x_{\text{bj}} f_{q/A}(x_{\text{bj}}, Q^2). \tag{A11}$$

Thus, we are able to simulate the DIS of LDM particles on nuclei in accordance with the calculated cross section. At this stage, we obtain virtual mediators with the corresponding kinematic parameters Q^2 and ν.

References

1. Lanfranchi, G.; Pospelov, M.; Schuster, P. The Search for Feebly-Interacting Particles. *arXiv* **2020**, arXiv:hep-ex/2011.02157.
2. Boehm, C.; Ascasibar, Y. More evidence in favor of light dark matter particles? *Phys. Rev. D* **2004**, *70*, 115013. [CrossRef]
3. Fabbrichesi, M.; Gabrielli, E.; Lanfranchi, G. The Dark Photon. *arXiv* **2005**, arXiv:hep-ex/2005.01515 [CrossRef]
4. Aguilar-Arevalo, A.; Brown, B.; Bugel, L.; Cheng, G.; Church, E.; Conrad, J.; Dharmapalan, R.; Djurcic, Z.; Finley, D.; Ford, R.; et al. Improved search for $\nu\ \mu \rightarrow \nu$ e oscillations in the MiniBooNE experiment. *Phys. Rev. Lett.* **2013**, *110*, 161801. [CrossRef] [PubMed]
5. Abe, K.; Abgrall, N.; Aihara, H.; Ajima, Y.; Albert, J.; Allan, D.; Amaudruz, P.A.; Andreopoulos, C.; Andrieu, B.; Anerella, M.; et al. The T2K experiment. *Nucl. Instrum. Methods Phys. Res. Sect. A Accel. Spectrometers Detect. Assoc. Equip.* **2011**, *659*, 106–135. [CrossRef]
6. SHiP Collaboration. A facility to Search for Hidden Particles (SHiP) at the CERN SPS. *arXiv* **2015**, arXiv:hep-ex/1504.04956.
7. Agafonova, N.; Aleksandrov, A.; Altinok, O.; Ambrosio, M.; Anokhina, A.; Aoki, S.; Ariga, A.; Ariga, T.; Autiero, D.; Badertscher, A.; et al. Observation of a first $\nu\tau$ candidate event in the OPERA experiment in the CNGS beam. *Phys. Lett. B* **2010**, *691*, 138–145. [CrossRef]
8. SHiP Collaboration. Sensitivity of the SHiP experiment to light dark matter. *arXiv* **2020**, arXiv:hep-ex/2010.11057.
9. Andreopoulos, C.; Barry, C.; Dytman, S.; Gallagher, H.; Golan, T.; Hatcher, R.; Perdue, G.; Yarba, J. The GENIE neutrino Monte Carlo generator: Physics and user manual. *arXiv* **2015**, arXiv:hep-ex/1510.05494.
10. Boehm, C.; Fayet, P. Scalar dark matter candidates. *Nucl. Phys. B* **2004**, *683*, 219–263. [CrossRef]
11. Pospelov, M.; Ritz, A.; Voloshin, M. Secluded WIMP dark matter. *Phys. Lett. B* **2008**, *662*, 53–61. [CrossRef]
12. Cline, J.M.; Dupuis, G.; Liu, Z.; Xue, W. The windows for kinetically mixed $Z^{'}$-mediated dark matter and the galactic center gamma ray excess. *J. High Energy Phys.* **2014**, *8*, 131. [CrossRef]
13. Buonocore, L.; Frugiuele, C.; Maltoni, F.; Mattelaer, O.; Tramontano, F. Event generation for beam dump experiments. *J. High Energy Phys.* **2019**, *2019*, 28. [CrossRef]
14. Deniverville, P.; Chen, C.Y.; Pospelov, M.; Ritz, A. Light dark matter in neutrino beams: Production modeling and scattering signatures at MiniBooNE, T2K, and SHiP. *Phys. Rev. D* **2017**, *95*, 035006. [CrossRef]
15. Shalaev, V.; Gorbunov, I.; Shmatov, S. Measurement of the Forward-Backward Asymmetry in the Drell-Yan Dilepton Production in Proton-Proton Collisions at the CMS Experiment at the LHC. In *EPJ Web of Conferences*; EDP Sciences: Les Ulis, France, 2018; Volume 177, p. 04010.
16. SHiP Collaboration. Sensitivity of the SHiP experiment to dark photons decaying to a pair of charged particles. *arXiv* **2020**, arXiv:hep-ex/2011.05115.
17. Nadolsky, P.M.; Lai, H.L.; Cao, Q.H.; Huston, J.; Pumplin, J.; Stump, D.; Tung, W.K.; Yuan, C.P. Implications of CTEQ global analysis for collider observables. *Phys. Rev. D* **2008**, *78*, 013004. [CrossRef]
18. Ahdida, C.; Akmete, A.; Albanese, R.; Alexandrov, A.; Andreini, M.; Anokhina, A.; Aoki, S.; Arduini, G.; Atkin, E.; Azorskiy, N.; et al. SND@ LHC. *arXiv* **2020**, arXiv:hep-ex/2002.08722.
19. Gninenko, S.; Kirpichnikov, D.; Kirsanov, M.; Krasnikov, N. The exact tree-level calculation of the dark photon production in high-energy electron scattering at the CERN SPS. *Phys. Lett. B* **2018**, *782*, 406–411. [CrossRef]
20. Sjostrand, T.; Mrenna, S.; Skands, P. PYTHIA 6.4 Physics and Manual. *J. High Energy Phys.* **2006**, *2006*. [CrossRef]
21. Soper, D.E.; Spannowsky, M.; Wallace, C.J.; Tait, T.M. Scattering of dark particles with light mediators. *Phys. Rev. D* **2014**, *90*, 115005. [CrossRef]

22. Yang, T.; Andreopoulos, C.; Gallagher, H.; Hofmann, K.; Kehayias, P. A hadronization model for few-GeV neutrino interactions. *Eur. Phys. J. C* **2009**, *63*, 1–10. [CrossRef]
23. Izaguirre, E.; Krnjaic, G.; Schuster, P.; Toro, N. Analyzing the Discovery Potential for Light Dark Matter. *Phys. Rev. Lett.* **2015**, *115*, 251301. [CrossRef] [PubMed]
24. Essig, R.; Mardon, J.; Papucci, M.; Volansky, T.; Zhong, Y.M. Constraining Light Dark Matter with Low-Energy e^+e^- Colliders. *J. High Energy Phys.* **2013**, *11*, 167. [CrossRef]
25. Pedregosa, F.; Varoquaux, G.; Gramfort, A.; Michel, V.; Thirion, B.; Grisel, O.; Blondel, M.; Prettenhofer, P.; Weiss, R.; Dubourg, V.; et al. Scikit-learn: Machine learning in Python. *J. Mach. Learn. Res.* **2011**, *12*, 2825–2830.
26. Ganapathi, A.; Kuno, H.; Dayal, U.; Wiener, J.L.; Fox, A.; Jordan, M.; Patterson, D. Predicting multiple metrics for queries: Better decisions enabled by machine learning. In Proceedings of the 2009 IEEE 25th International Conference on Data Engineering, Shanghai, China, 29 March–2 April 2009; pp. 592–603.
27. Okun', L. *Leptons and Quarks*; URSS: Moscow, Russia, 2005.
28. Grozin, A. *Solution of Physical Problems with REDUCE*; Technical Report; AN SSSR: Moscow, Russia, 1988.
29. Hirai, M.; Kumano, S.; Nagai, T.H. Determination of nuclear parton distribution functions and their uncertainties at next-to-leading order. *Phys. Rev. C* **2007**, *76*. [CrossRef]